ACS OMEGA

http://pubs.acs.org/journal/acsodf

Article

# Intracluster Reaction Dynamics of Ionized Micro-Hydrated Hydrogen Peroxide ($H_2O_2$): A Direct Ab Initio Molecular Dynamics Study

Shuhei Yamasaki and Hiroto Tachikawa*

Cite This: *ACS Omega* 2022, 7, 33866−33872

Read Online

ACCESS | Metrics & More | Article Recommendations | Supporting Information

**ABSTRACT:** Hydrogen peroxide ($H_2O_2$) is a unique molecule that is applied in various fields, including energy chemistry, astrophysics, and medicine. $H_2O_2$ readily forms clusters with water molecules. In the present study, the reactions of ionized $H_2O_2$−water clusters, $H_2O_2^+(H_2O)_n$, after vertical ionization of the parent neutral cluster were investigated using the direct ab initio molecular dynamics (AIMD) method to elucidate the reaction mechanism. Clusters with one to five water molecules, $H_2O_2$−$(H_2O)_n$ ($n$ = 1−5), were examined, and the reaction of $[H_2O_2^+(H_2O)_n]_{ver}$ was tracked from the vertical ionization point to the product state, where $[H_2O_2^+(H_2O)_n]_{ver}$ is the vertical ionization state (hole is localized on $H_2O_2$). After ionization, fast proton transfer (PT) from $H_2O_2^+$ to the water cluster $(H_2O)_n$ was observed in all clusters. The HOO radical and $H_3O^+(H_2O)_{n-1}$ were formed as products. The PT reaction proceeds directly without an activation barrier. The PT times for $n$ = 1−5 were calculated to be 36.0, 9.8, 8.3, 7.7, and 7.1 fs, respectively, at the MP2/6-311++G(d,p) level, indicating that PT in these clusters is a very fast process, and the PT time is not dependent on the cluster size ($n$), except in the case of $n$ = 1, where the PT time was slightly longer because the bond distance and angle of the hydrogen bond in $n$ = 1 were deformed from the standard structure. The reaction mechanism was discussed based on these results.

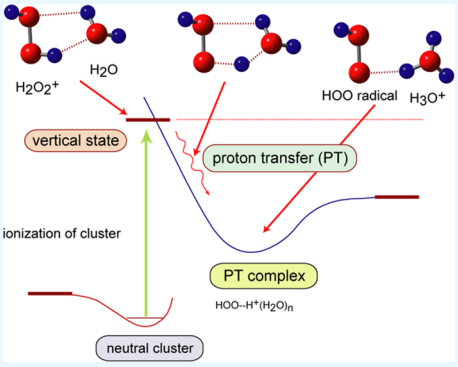


## 1. INTRODUCTION

Hydrogen peroxide ($H_2O_2$) is a unique molecule that is applied in various fields. In the field of energy chemistry, $H_2O_2$ serves as a safe and clean hydrogen carrier molecule.[1−4] Hydrogen molecule ($H_2$) can be extracted easily from $H_2O_2$ under the action of a catalyst by visible-light irradiation.[1] Recently, Shiraishi et al. showed that $H_2$ molecules can be produced from $H_2O_2$ by photo-irradiation.[5] Photoirradiation of $H_2O_2$ under catalytic conditions efficiently produces $H_2$. This method is expected to be effective for $H_2$ production in spacecraft and space stations because $H_2O_2$ can be used to produce $H_2$ under mild conditions.

$H_2O_2$ is a well-known molecule in medicine and is commonly used as a disinfectant. Recently, hydrogen peroxide water ($H_2O_2$−$H_2O$) achieved breakthrough results in radiotherapy. Nimalasena et al. reported a rapid increase in the cancer recovery rate after radiotherapy by injecting $H_2O_2$−$H_2O$ into tumor areas.[6] Thus, $H_2O_2$−$H_2O$ has potential as a radiation response enhancer in cancers for which conventional radiotherapy is insufficient for local control. However, its mechanism has not been elucidated thus far; the ionization and electron capture reactions of $H_2O_2$−$H_2O$ clusters may be responsible for the initial reaction processes after irradiation.

Additionally, $H_2O_2$ has been observed in space, where radiation and cosmic rays are emitted. A European research group observed a molecular cloud in Ophiuchus (Oph), and $H_2O_2$ was detected in the cloud core of $\rho$ Oph-A.[7] Notably, $H_2O_2$ is an essential molecule for producing water in space and forms clusters with $H_2O$.[8,9] However, no study on the effects of cosmic ray irradiation on the reactions of $H_2O_2$−$H_2O$ clusters has been reported to date.

The simplest reaction of $H_2O_2$ without $H_2O$ in Earth is its photolysis under UV light. From the perspective of atmospheric chemistry, Kawasaki and co-workers measured the Doppler profiles of H atoms formed from the photodissociation of $H_2O_2$ at 193 nm using a laser-induced fluorescence method.[10,11] They suggested that the excited state of $H_2O_2$ ($A^1A$) is responsible for H atom formation from $H_2O_2$. Thus, photoreactions of $H_2O_2$ have been extensively investigated.[12−14] However, information on the reaction of micro-solvated $H_2O_2$ is limited. In particular, reactions involving the ionized state of micro-solvated $H_2O_2$ are scarcely known.

In the present study, the reactions of ionized hydrogen peroxide−water clusters, denoted as $[H_2O_2$−$(H_2O)_n]^+$, after vertical ionization of neutral cluster, are investigated using the

Received: May 2, 2022
Accepted: September 6, 2022
Published: September 15, 2022

© 2022 The Authors. Published by American Chemical Society



https://doi.org/10.1021/acsomega.2c02730
*ACS Omega* 2022, 7, 33866−33872

direct ab initio molecular dynamics (MD) method[15−17] to elucidate the effects of micro-solvation on the reaction of $H_2O_2$. Clusters with one to five water molecules, $H_2O_2$−$(H_2O)_n$ ($n$ = 1−5), are examined.

Previously, the structures of micro-solvated $H_2O_2$ (neutral state) were determined using ab initio calculations. Kulkarni et al. investigated the structures and binding energies of $H_2O_2$−$(H_2O)_n$ ($n$ = 1−6).[18] The binding energy of the $H_2O_2$−$H_2O$ 1:1 complex was calculated to be 7.4−11.2 kcal/mol, which is larger than the hydrogen bonding energy of the water dimer (5.0−6.0 kcal/mol). They found several conformers of the clusters. The ionization and excitation energies were calculated by Ferreira et al.[19] They showed that these energies are not dependent on the size of the cluster because the excitation and ionization are localized on $H_2O_2$ in the clusters. Thus, the ionized states of the clusters were investigated only for static states. The reactions of the ionized states of the clusters were not calculated. In this study, we focus on the reaction dynamics of the ionized states of the clusters.

## 2. COMPUTATIONAL DETAILS

**2.1. Ab Initio Calculations.** The geometries of the neutral clusters, $H_2O_2(H_2O)_n$ ($n$ = 1−5), were optimized using the second-order perturbation Møller−Plesset (MP2) method with the 6-311++G(d,p) basis set.[20,21] In addition, the CAM-B3LYP functional was also utilized.[22] The coupled-cluster single, double, and perturbative triple excitation (CCSD(T)) method[23] was used for small clusters ($n$ = 1 and 2). For $n$ = 1−3, quadratic configuration interaction with singles and doubles (QCISD)[24] and fourth-order MP theory correction including the single, double, and quadruple substitution MP4(SDQ) method[25] were used to determine the structures of the clusters. The atomic and molecular charges were calculated using the natural population analysis (NPA) approach. Standard Gaussian 09 and 16 program packages were used for all static *ab initio* calculations.[26,27]

**2.2. Direct AIMD Calculations.** Two methods were used in the direct ab initio molecular dynamics (AIMD) calculations using: (a) the optimized structure of the neutral cluster as a starting structure and (b) the zero-point vibrational energy (ZPE). The NVE ensemble (microcanonical ensemble) was employed. In the direct AIMD calculation of the optimized structure, neutral clusters, $H_2O_2(H_2O)_n$, were first optimized at the MP2/6-311++G(d,p) level. Thereafter, the trajectory of $H_2O_2^+$−$(H_2O)_n$ was started from the vertical ionization point. The rotational temperature, momentum vector, and excess energy of $[H_2O_2^+$−$(H_2O)_n]_{ver}$ were set to be zero (time = 0 fs). The maximum simulation time was 2.1 ps. A time step was 0.10 fs. The velocity Verlet algorithm was utilized to solve the equations of motion for the system. The drift of total energy was less than 0.01 kcal/mol. Similar calculations were performed using the CAM-B3LYP functional.

The effects of ZPE on the reaction mechanism were investigated using the classical vibrational sampling method (microcanonical ensemble).[28−30] The effects of the functional on the reaction mechanism were investigated using the ωB97XD functional[31] and compared with those obtained with the CAM-B3LYP functional. Direct AIMD calculations were carried out using our own code.[15−17]

## 3. RESULTS

**3.1. Structures of $H_2O_2(H_2O)_n$ ($n$ = 1−5).** The optimized structure of the $H_2O_2$−$H_2O$ 1:1 neutral complex is shown in Figure 1 ($n$ = 1). In this structure, one of the protons of $H_2O_2$ (H1) is oriented toward the oxygen atom of $H_2O$, and the oxygen atom of $H_2O_2$ (O2) accepts a proton from $H_2O$.

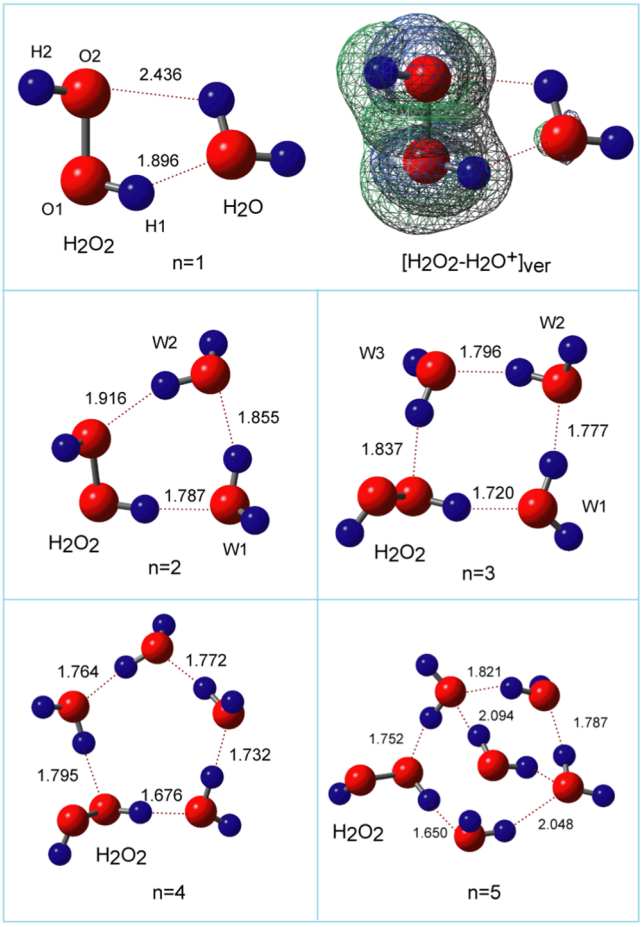


**Figure 1.** Optimized structures of $H_2O_2(H_2O)_n$ neutral clusters ($n$ = 1−5). Spatial distribution shows the spin density of vertical ionization state, $[H_2O_2$−$H_2O^+]_{ver}$. The calculations were carried out at the MP2/6-311++G(d,p) level. Bond lengths are in Å.

The spatial distribution of the spin density of $[H_2O_2^+$−$H_2O^+]_{ver}$ for the ionization state is illustrated in Figure 1 ($n$ = 1, right), where $[H_2O_2^+$−$H_2O]_{ver}$ indicates the vertical ionization state of $H_2O_2$−$H_2O$. The molecular spin densities of $H_2O_2$ and $H_2O$ were calculated to be 0.999 and 0.001, respectively, implying that the unpaired electrons (holes) are fully localized on $H_2O_2$. The spin densities of the hydroxyl groups (H1O1) and (O2H2) of $[H_2O_2$−$H_2O^+]_{ver}$ were +1.180 and −0.179, respectively, suggesting that the spin density on the OH group (H1O1) is induced by the interaction with $H_2O$. The spin densities of the OH groups of free $H_2O_2^+$ (without $H_2O$) were calculated as (H1O1) = 0.500 and (O2H2) = 0.500.

The optimized structure of $H_2O_2(H_2O)_n$ ($n$ = 2) and spatial distribution of the spin density of $[H_2O_2(H_2O)_2^+]_{ver}$ are illustrated in Figure 1 ($n$ = 2) and Figure S1 ($n$ = 2), respectively. In this structure, the water dimer is oriented toward $H_2O_2$ with two hydrogen bonds. The hydrogen bond



https://doi.org/10.1021/acsomega.2c02730
ACS Omega 2022, 7, 33866−33872

distances are 1.787 Å (W1) and 1.916 Å (W2), which are significantly shorter than those of the 1:1 complex (1.896 and 2.436 Å for $n$ = 1).

In the vertical ionization state, the molecular spin densities of $H_2O_2$, W1, and W2 were calculated to be 1.001, 0.005, and −0.006, respectively, indicating that the unpaired electron is localized on $H_2O_2$. The spin densities of the OH groups of $H_2O_2$ for $n$ = 2 were 0.576 and 0.426, respectively, indicating that water molecules induced slight polarization of the spin densities on $(H_2O_2)^+$.

The optimized structures for $n$ = 3−5 are given in Figure 1 ($n$ = 3−5), and the spin density distributions are shown in Figure S1. The NPA charges are listed in Table S1 (MP2) and Table S2 (CAM-B3LYP). In all of the clusters, the spin densities were mainly localized on the $H_2O_2$ moiety of the $[H_2O_2^+(H_2O)_n]_{ver}$ ($n$ = 3−5) clusters. The spin densities on $H_2O$ (the MP2 values) were 0.971 ($n$ = 3), 0.969 ($n$ = 4), and 0.946 ($n$ = 5). This trend is because the ionization energy of $H_2O_2$ (10.5 eV) is lower than that of $H_2O$ (12.6 eV).[32,33] Moreover, spin polarization was observed in all cluster cations. The optimized structures of the neutral clusters are in good agreement with previous calculations.[18,19]

**3.2. Reaction Dynamics of $H_2O_2^+$−$H_2O$ after Ionization.** In this section, the reaction following the ionization of the parent neutral complex is considered. The potential energy of $[H_2O_2^+$−$H_2O]$, following ionization, was plotted as a function of time, as shown in Figure 2A.

The zero energy level adopts the total energy of the vertical ionization point. Figure 2B presents snapshots of $H_2O_2^+$−$H_2O$ over time. The spin densities of $H_2O_2$ and $H_2O$ were 0.999 and 0.001, respectively, at time zero, indicating that the holes were localized on $H_2O_2$. The H1 proton was located at $r1$ = 1.896 and $r2$ = 0.973 Å at time zero, denoted as ($r1$, $r2$) = (1.896, 0.973). The potential energy decreased suddenly after ionization. This is due to rapid proton transfer (PT) from $H_2O_2^+$ to $H_2O$: the H1 proton was located in the central region between $H_2O_2$ and $H_2O$ at 27.5 fs with (1.223, 1.241) and (1.011, 1.164) at 37.9 fs. PT occurred immediately, and a radical-ion complex, $HOO^-(H_3O^+)$, was formed. At 50.1 fs, the complex underwent structural relaxation. The potential energy was the lowest at 50.1 fs, where the stable complex $HOO-(H_3O^+)$ was formed. A short time later, the complex dissociated into the HOO radical and $H_3O^+$, as shown in the snapshot at 200 fs.

**3.3. Reaction Dynamics of $H_2O_2^+(H_2O)_n^+$ ($n$ = 2) after Ionization.** The time evolution of potential energy and snapshots of $[H_2O_2^+(H_2O)_2]$, following the vertical ionization, are shown in Figure 3A.

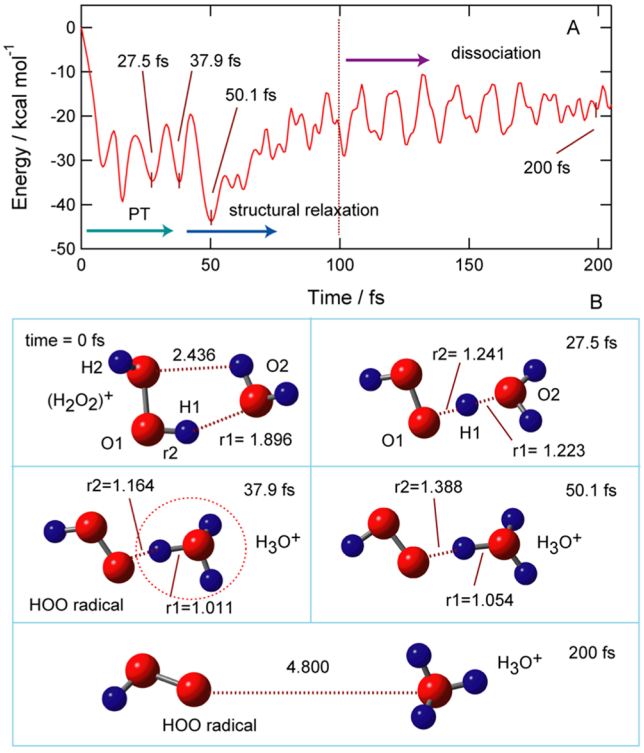


**Figure 2.** Time evolution of (A) potential energy and (B) snapshots of the $H_2O_2-(H_2O)_n^+$ reaction system ($n$ = 1) after ionization of the parent neutral cluster. Direct AIMD calculation was performed at the MP2/6-311++G(d,p) level. The MP/6-311++G(d,p)-optimized geometry was used as the initial geometry of $[H_2O_2-H_2O^+]_{ver}$ at time zero.

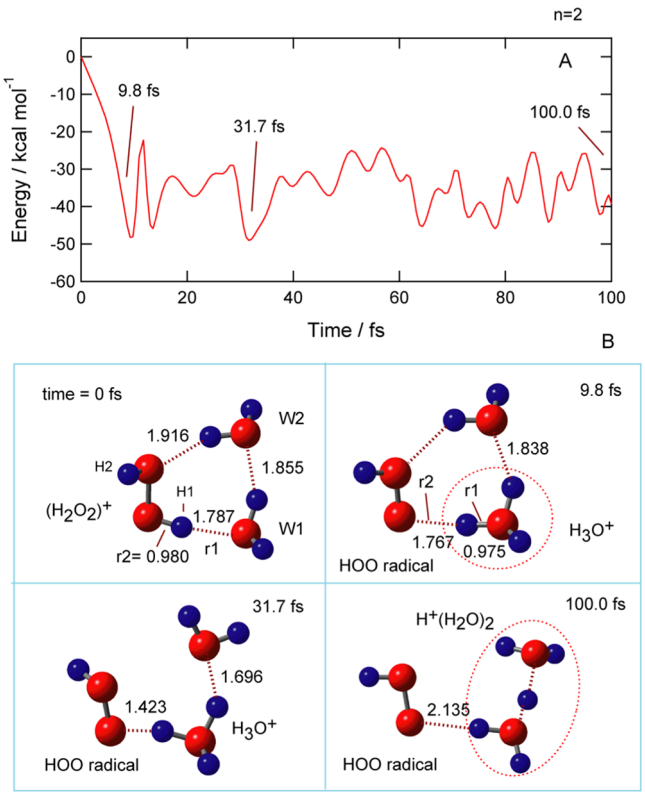


**Figure 3.** Time evolution of (A) potential energy and (B) snapshots of the $H_2O_2-(H_2O)_n^+$ reaction system ($n$ = 2) after ionization of the parent neutral cluster. Direct AIMD calculation was performed at the MP2/6-311++G(d,p) level. The MP/6-311++G(d,p)-optimized geometry was used as the initial geometry of $[H_2O_2-(H_2O)_2^+]_{ver}$ at time zero.

The spin densities of $H_2O_2$, W1, and W2 at the vertical ionization point were 1.001, 0.005, and −0.006, respectively, suggesting that the unpaired electron is localized on $H_2O_2$, similar to the case for $n$ = 1. In $H_2O_2^+$, the spin density of the hydroxyl group with the proton donor (density = 0.579) was larger than that of the other group (density = 0.426). After ionization, the H1 proton underwent rapid PT from $H_2O_2^+$ to $H_2O$, which generated $H_3O^+$. At time = 9.8 fs, H1 was located


https://doi.org/10.1021/acsomega.2c02730
ACS Omega 2022, 7, 33866−33872

at ($r1$, $r2$) = (0.975, 1.767), indicating that PT was completed and was significantly fast. The energy declined rapidly to −50.0 kcal at 9.8 fs. Structural relaxation within the HOO−$H^+(H_2O)_2$ cluster occurred immediately, as observed at time = 31.7 fs. In the final stage of the reaction, a Zundel complex composed of $H^+(H_2O)_2$ was formed, which interacted weakly with the HOO radical. In the case of $n$ = 2, dissociation of the HOO radical was not observed and the complex remained in the reaction field.

**3.4. Reaction Dynamics of $H_2O_2^+(H_2O)_n$ ($n$ = 3−5) after Ionization.** The same calculations were performed for larger clusters, $[H_2O_2^+(H_2O)_n]$ ($n$ = 3−5). The results are shown in Figure S2 ($n$ = 3), Figure S3 ($n$ = 4), and Figure S4 ($n$ = 5). The calculated PT times for $n$ = 3, 4, and 5 were 8.3, 7.7, and 7.1 fs, respectively, at the MP2/6-311++G(d,p) level of theory. Similar calculations were performed at the CAM-B3LYP/6-311++G(d,p) level. The calculated PT times for $n$ = 1−5 were 26.8, 10.4, 8.8, 7.7, and 7.1 fs, respectively, at the CAM-B3LYP/6-311++G(d,p) level. The PT times obtained using MP2 and CAM-B3LYP are summarized in Figure 4.

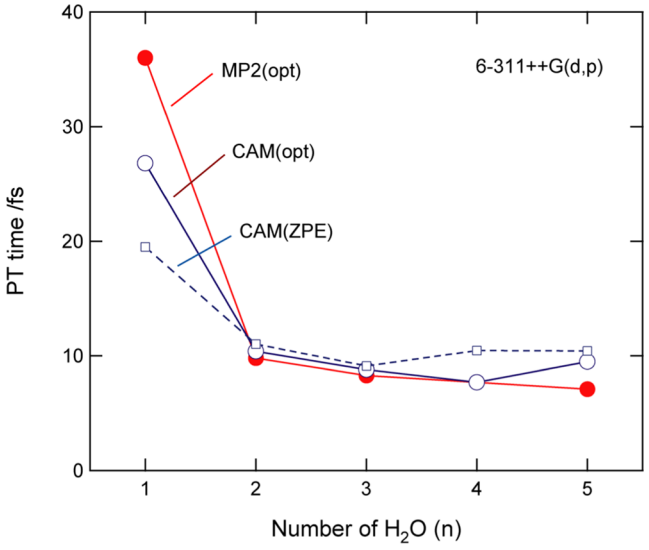


**Figure 4.** Proton transfer (PT) time for $H_2O_2$−$(H_2O)_n^+$, following vertical ionization of neutral cluster, plotted as a function of cluster size ($n$). MP2(opt) indicates that the MP/6-311++G(d,p)-optimized geometry was used as the initial geometry of $[H_2O_2$−$(H_2O)_n^+]_{ver}$ at time zero, and direct AIMD calculation was carried out at the MP2/6-311++G(d,p) level. CAM(opt) indicates that the CAM-B3LYP/6-311++G(d,p)-optimized geometry was used as the initial geometry of $[H_2O_2$−$(H_2O)_n^+]_{ver}$ at time zero, and direct AIMD calculation was carried out at the CAM-B3LYP/6-311++G(d,p) level. CAM(ZPE) indicates that direct AIMD calculations were carried out, including zero-point vibrational energies (ZPEs); average PT times are shown.

As clearly seen in this figure, the trends and values obtained at both levels of theory (MP2 and CAM-B3LYP) are in excellent agreement with each other. The PT time for $n$ = 1 was slightly longer than that for the other clusters, whereas the PT times for $n$ = 2−5 were almost constant (7−11 fs). This trend is consistent for both methods. The observations will be explained in Section 4.

**3.5. Effects of Zero-Point Vibrational Energy (ZPE) on the Reaction Mechanism.** In this section, the effects of the zero-point energy (ZPE) on the PT time are examined. All calculations were performed at the CAM-B3LYP/6-311++G(d,p) level of theory. First, the geometries of $H_2O_2(H_2O)_n$ ($n$ = 1−5) were optimized. Thereafter, the zero-point vibrational energy (ZPE) was applied to $H_2O_2(H_2O)_n$. The microcanonical ensemble of classical harmonic vibrations in the sampling method was applied to the reaction system.[28−30] All atoms in the initial state of $[H_2O_2^+(H_2O)_n^+]_{ver}$ had momenta corresponding to their vibrational energies. Direct AIMD calculations were carried out for $n$ = 1−5. Ten trajectories were performed for each cluster size ($n$). The time evolution of the potential energy of $H_2O_2^+(H_2O)_n$, following ionization of the $H_2O_2$−$H_2O$ 1:1 complex, including the ZPE, is plotted in Figure 5.

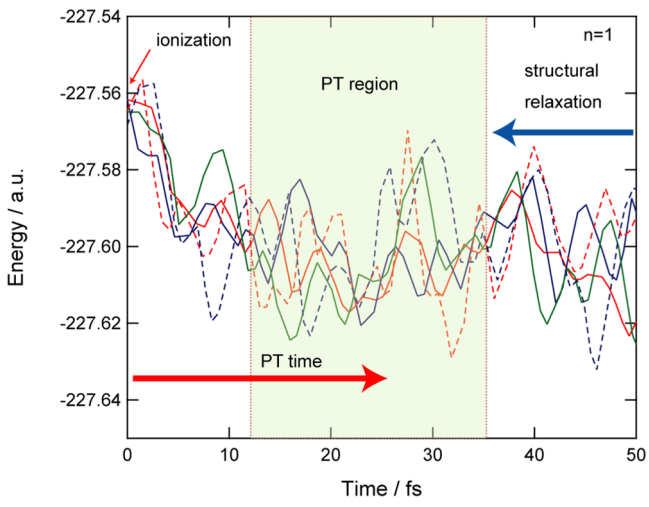


**Figure 5.** Effects of ZPE on the time evolution of the potential energy for $n$ = 1 (five trajectories are given). Direct AIMD calculation was performed at the CAM-B3LYP/6-311++G(d,p) level.

Five trajectories are shown as a sample. After ionization, the potential energy decreased rapidly, and PT rapidly ensued. The PT time was distributed in the range of 12.4−35.8 fs, where the average PT time was 19.5 fs for $n$ = 1. After PT, the structure of the complex was energetically relaxed.

The same calculations were carried out for $n$ = 2−5. The results are shown in Figures S5 and S6. Similar PT was also observed. The average PT time is shown in Figure 4 (denoted as CAM(ZPE)). The average PT times for $n$ = 1−5 were 19.5, 11.0, 9.1, 10.5, and 10.4 fs, respectively. Considering the ZPE, the PT time was the longest for $n$ = 1. This trend is the same as that in the case without the zero-point vibrational energy. In the case of $n$ = 1, the PT time was 19.5 fs (ZPE) and 26.8 fs (no-ZPE), indicating that the ZPE slightly accelerates the PT time.

**3.6. Potential Energy Curves for the Reaction System.** As a summary of the present calculations, a schematic illustration of the potential energy curves for the reaction system is given in Figure 6.

The relative energies are listed in Table S3 (MP2) and Table S4 (CAM-B3LYP). After the ionization of $H_2O_2(H_2O)_n$, the reaction point shifted toward the vertical ionization state, termed "vertical state". PT occurred immediately to generate the PT complex, HOO−$H^+(H_2O)_n$. PT in the present reaction system is a very fast process because the reaction proceeds without a barrier and has a large excess energy. The PT times for $n$ = 1−5 were 36.0, 9.8, 8.3, 7.7, and 7.1 fs, respectively, at the MP2/6-311++G(d,p) level. Although the energy level of


https://doi.org/10.1021/acsomega.2c02730
ACS Omega 2022, 7, 33866−33872

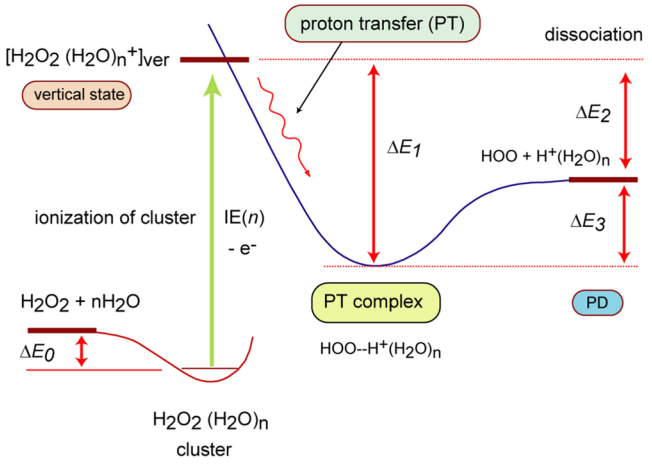


**Figure 6.** Energy diagram for the reaction system. IE means ionization energy of clusters.

the product state (PD) is lower than that of the vertical state, dissociation to HOO + $H^+(H_2O)_n$ occurred only for $n$ = 1 due to the fact the large number of degrees of freedom in $n$ = 2−5 prevents dissociation. The excess energy of the PT complex is dissipated efficiently into the vibrational modes of the PT complex.

The optimized structures of the PT complexes are shown in Figure S7 together with those obtained by direct AIMD calculations. The structures of PT complex obtained from direct AIMD calculation and geometry optimization were similar to each other: the structure is composed of HOO radical and $H_3O^+$ in both cases.

The dissociation energy for the reaction ($\Delta E3$), HOO═$H^+(H_2O)_n$ → HOO + $H^+(H_2O)_n$, becomes smaller in larger clusters. However, the dissociation was not found within this time scale. This is due to the fact that large degrees of freedom prevent the dissociation in larger clusters ($n$ = 3−5). Namely, the excess energy was efficiently transferred into the internal modes of clusters (the stretching vibrational and bending modes)

**3.7. Effects of Functional and Initial Geometries on Reaction Mechanism.** The direct AIMD calculations in the previous sections were carried out using the MP2 and DFT methods (CAM-B3LYP functional), starting from the initial geometry obtained by each method. The effects of the functional (ωB97XD) and initial geometries on the reaction mechanism are discussed in this section. The initial geometries were calculated at the ωB97XD, QCISD, and CCSD/6-311++G(d,p) levels of theory, and direct AIMD calculations were performed for each geometry. The obtained PT times are listed in Table 1.

At all levels of theory, the PT time for $n$ = 1 was longer than that for $n$ = 2, and the results were independent of the method used.

## 4. DISCUSSION AND CONCLUSIONS

The present calculations show that vertically ionized cluster cations can undergo PT as an intracluster reaction. The PT time for $n$ = 1 is slightly longer than that for $n$ = 2−5 (36.0 fs for $n$ = 1 and 9.8 fs for $n$ = 2). This difference arises because the bond distance and angle of the hydrogen-bond structure in $n$ = 1 deviate from the standard hydrogen bond, as shown in Figure S8. In the water dimer, the distance and angle are 1.950 Å and 176.8°, respectively, and 1.787 Å and 168.7° for $H_2O_2$−$H_2O$ in $n$ = 2. In contrast, the corresponding values are 1.896 Å and 148.5° in the $H_2O_2$−$H_2O$ 1:1 complex ($n$ = 1), deviating from the normal hydrogen bonds appearing in $n$ = 2−5 and in the water dimer. The angle of the hydrogen bond (O−H═H) at $n$ = 1 is largely distorted from the normal collinear form. This difference leads to a longer PT time for $n$ = 1.

**Table 1. Effects of Initial Geometry and Functional on PT Time (in fs)[a]**

| geometry | AIMD | $n$ = 1 | $n$ = 2 | $n$ = 3 |
|---|---|---|---|---|
| MP2 | MP2 | 36.0 | 9.8 | 8.3 |
| CAM-B3LYP | CAM-B3LYP | 26.8 | 10.4 | 8.8 |
| ωB97XD | ωB97XD | 32.6 | 12.2 | 9.3 |
| MP4SDQ | MP2 | 34.0 | 10.5 | 9.1 |
| QCISD | MP2 | 34.1 | 10.6 | 9.1 |
| CCSD | MP2 | 34.2 | 10.6 | not calc. |

[a]"Geometry" indicates the method of calculation used to obtain the initial geometry (time = 0 fs), and "AIMD" refers to direct AIMD calculation. The 6-311++G(d,p) basis set was used in all calculations.

In the present study, several approximations were introduced in the calculations. In the direct AIMD calculations, the normal mode sampling method was used in the initial sampling using ZPEs and the quantum effects of nuclear motion were neglected.[34,35] The Wigner phase-space sampling method is more accurate for the initial sampling. However, these effects on the reaction mechanism are minimal because the present reaction system is composed of a simple repulsive dissociation surface.

The number of trajectories used in the calculations was limited because the direct AIMD calculation at the MP2/6-311++G(d,p) level required a significant amount of central processing unit (CPU) time; only 10 trajectories were run for each cluster.

The PT time with error bars is shown in Figure S9, and wide error bars (standard deviation) were observed. Especially, the error bar in $n$ = 1 was larger than the others. If more accurate PT time is required, an increase in the number of calculations is necessary. Although several approximations were used in this study, the direct AIMD method can provide useful information regarding the reaction dynamics of $H_2O_2$−$H_2O$ ion clusters.

In space, $H_2O_2$ is electronically excited by UV irradiation, producing a reactive HOO radical and hydrogen atom. At even higher excitation energies, $H_2O_2$ is ionized. In the micro-hydrated $H_2O_2$, UV and cosmic ray irradiation ionizes the $H_2O_2$ moiety of the $H_2O_2$−$(H_2O)_n$ cluster, as expressed by eq 1. The present study shows that PT from $H_2O_2^+$ to the water clusters occurs after ionization, as shown in eq 2. The reactions are expressed by the following equations

$$H_2O_2 - (H_2O)_n + \text{cos mic} - \text{ray} \rightarrow (H_2O_2)^+(H_2O)_n + e^- \quad (1)$$

$$(H_2O_2)^+(H_2O)_n \rightarrow HOO - (H)^+(H_2O)_n \quad (2)$$

The PT process was extremely fast (~10 fs for $n$ = 2−5). Thus, the reaction mechanism of hydrated $H_2O_2^+$ after ionization of the neutral cluster was proposed in this study.



https://doi.org/10.1021/acsomega.2c02730
ACS Omega 2022, 7, 33866−33872

## ■ ASSOCIATED CONTENT

### Supporting Information

The Supporting Information is available free of charge at https://pubs.acs.org/doi/10.1021/acsomega.2c02730.

Optimized structures of $H_2O_2(H_2O)_n$ neutral clusters ($n$ = 1−5), time evolution of potential energy of $H_2O_2(H_2O)_n^+$ ($n$ = 3, 4, and 5), snapshots, effects of ZPE on the time evolution of potential energies for $n$ = 2 and 3, time evolution of distances and angles of hydrogen bond between $H_2O_2$ and $H_2O$, spin densities and NPA molecular charges on $H_2O_2$ and $(H_2O)_n$, hydration energies of $H_2O_2$, relaxation energies, and reaction energies, and dissociation energies (PDF)

## ■ AUTHOR INFORMATION


### Corresponding Author

**Hiroto Tachikawa** − *Division of Applied Chemistry, Graduate School of Engineering, Hokkaido University, Sapporo 060-8628, Japan;* orcid.org/0000-0002-7883-2865; Email: hiroto@eng.hokudai.ac.jp

### Author

**Shuhei Yamasaki** − *Department of Applied Chemistry and Biochemistry, National Institute of Technology, Wakayama College, Gobo, Wakayama 644-0023, Japan*

Complete contact information is available at: https://pubs.acs.org/10.1021/acsomega.2c02730


### Notes

The authors declare no competing financial interest.

## ■ ACKNOWLEDGMENTS

The authors acknowledge partial support from JSPS KAKENHI (Grant Numbers 21H05415 and 21K04973).

## ■ REFERENCES


(1) Shiraishi, Y.; Matsumoto, M.; Ichikawa, S.; Tanaka, S.; Hirai, H. Polythiophene-Doped Resorcinol−Formaldehyde Resin Photocatalysts for Solar-to-Hydrogen Peroxide Energy Conversion. *J. Am. Chem. Soc.* **2021**, *143*, 12590−12599.

(2) Liu, T.; Pan, Z.; Vequizo, J. J. M.; Kato, K.; Wu, B.; Yamakata, K.; Katayama, K.; Chen, B.; Chen, B.; Chu, C.; Chu, C.; Domen, K. Overall Photosynthesis of $H_2O_2$ by an Inorganic Semiconductor. *Nat. Commun.* **2022**, *13*, No. 1034.

(3) Tachikawa, H. Formation of Hydrogen Peroxide from $O^-(H_2O)_n$ Clusters. *J. Phys. Chem. A* **2021**, *125*, 4598−4605.

(4) Kou, M.; Wang, Y.; Xu, Y.; Ye, L.; Huang, Y.; Jia, B.; Li, H.; Ren, J.; Deng, Y.; Chen, J.; Zhou, Y.; Lei, K.; Wang, L.; Liu, W.; Huang, H.; Ma, T. Molecularly Engineered Covalent Organic Frameworks for Hydrogen Peroxide Photosynthesis. *Angew. Chem., Int. Ed.* **2022**, *61*, No. e202200413.

(5) Shiraishi, Y.; Ueda, Y.; Soramoto; Hinokuma, S.; Hirai, T. Photocatalytic Hydrogen Peroxide Splitting on Metal-Free Powders Assisted by Phosphoric Acid as a Stabilizer. *Nat. Commun.* **2020**, *11*, No. 3386.

(6) Nimalasena, S.; Gothard, L.; Anbalagan, S.; Allen, S.; Sinnett, V. Mohammed, K.; Kothari, G., Intratumoral Hydrogen Peroxide With Radiation Therapy in Locally Advanced Breast Cancer: Results From a Phase 1 Clinical Trial. *Int. J. Radiat. Oncol. Biol. Phys.* **2020**, *108*, 1019−1029.

(7) Bergman, P.; Parise, B.; Liseau, R.; Larsson, B.; Olofsson, H.; Menten, K. M.; Gusten, R. Detection of interstellar hydrogen peroxide. *A&A* **2011**, *531*, L8.

(8) Miyauchi, N.; Hidaka, H.; Chigai, T.; Nagaoka, A.; Watanabe, N.; Kouchi, A. Formation of hydrogen peroxide and water from the reaction of cold hydrogen atoms with solid oxygen at 10 K. *Chem. Phys. Lett.* **2008**, *456*, 27−30.

(9) Ioppolo, S.; Cuppen, H. M.; Romanzin, C.; van Dishoeck, E. F.; Linnartz, H. Laboratory Evidence for Efficient Water Formation in Interstellar Ices. *Astrophys. J.* **2008**, *686*, 1474−1479.

(10) Inagaki, Y.; Matsumi, Y.; Kawasaki, M. Formation of a Hydrogen Atom from the Photodissociation of Hydrogen Peroxide at 193 nm. *Bull. Chem. Soc. Jpn.* **1993**, *66*, 3166−3170.

(11) Yoshihara, K.; Sakamoto, Y.; Kawasaki, M.; Takatori, Y.; Kato, K.; Kajii, Y. UV-Light-Induced Water Condensation in Air and the Role of Hydrogen Peroxide. *Bull. Chem. Soc. Jpn.* **2014**, *87*, 593−602.

(12) Park, S. M.; Kang, C. M.; Kwon, C. H.; Kim, H. L. Dynamics of H Atom Production from Photodissociation of $H_2O_2$ at 205nm. *Chem. Phys. Lett.* **2014**, *592*, 124−126.

(13) Thiebaud, J.; Aluculesei, A.; Fittschen, C. Formation of $HO_2$ Radicals from the Photodissociation of $H_2O_2$ at 248nm. *J. Chem. Phys.* **2007**, *126*, No. 186101.

(14) Nakayama, T.; Takahashi, K.; Matsumi, Y. Quantum Yield for hydrogen Atom Formation from $H_2O_2$ Photolysis in the Range 193−240 nm. *Int. J. Chem. Kinet.* **2005**, *37*, 751−754.

(15) Tachikawa, H. Reaction Mechanism of an Intracluster $S_N2$ Reaction Induced by Electron Capture. *Phys. Chem. Chem. Phys.* **2022**, *24*, 3941−3950.

(16) Tachikawa, H. Reaction Dynamics of $NO^+$ with Water Clusters. *J. Phys. Chem. A* **2022**, *126*, 119−124.

(17) Tachikawa, H. Reactions of Photoionization-Induced CO−$H_2O$ Cluster: Direct Ab Initio Molecular Dynamics Study. *ACS Omega* **2021**, *6*, 16688−16695.

(18) Kulkarni, A. D.; Pathak, R. K.; Bartolotti, L. J. Structures, Energetics, and Vibrational Spectra of $H_2O_2\cdots(H_2O)$n, n = 1−6 Clusters: Ab Initio Quantum Chemical Investigations. *J. Phys. Chem. A* **2005**, *109*, 4583−4590.

(19) Ferreira, C.; Martinianno, H. F. M. C.; Costa Cabral, B. J.; Aquilant, V. Electronic Excitation and Ionization of Hydrogen Peroxide-Water Clusters: Comparison With Water Clusters. *Int. J. Quantum Chem.* **2011**, *111*, 1824−1835.

(20) McLean, A. D.; Chandler, G. S. Contracted Gaussian-Basis Sets for Molecular Calculations. I. Second Row Atoms, Z = 11-18. *J. Chem. Phys.* **1980**, *72*, 5639−5648.

(21) Head-Gordon, M.; Head-Gordon, T. Analytic MP2 Frequencies Without Fifth Order Storage: Theory and Application to Bifurcated Hydrogen Bonds in the Water Hexamer. *Chem. Phys. Lett.* **1994**, *220*, 122−128.

(22) Yanai, T.; Tew, D.; Handy, N. A new hybrid exchange-correlation functional using the Coulomb-attenuating method (CAM-B3LYP). *Chem. Phys. Lett.* **2004**, *393*, 51−57.

(23) Watts, J. D.; Gauss, J.; Bartlett, R. J. Coupled-cluster methods with noniterative triple excitations for restricted open-shell Hartree-Fock and other general single determinant reference functions. Energies and analytical gradients. *J. Chem. Phys.* **1993**, *98*, 8718−8733.

(24) Salter, E. A.; Trucks, G. W.; Bartlett, R. J. Analytic Energy Derivatives in Many-Body Methods. I. First Derivatives. *J. Chem. Phys.* **1989**, *90*, 1752−1766.

(25) Raghavachari, K.; Frisch, M. J.; Pople, J. A. Contribution of triple substitutions to the electron correlation energy in fourth-order perturbation theory. *Chem. Phys. Lett.* **1980**, *72*, 4244−4245.

(26) Frisch, M. J.; Trucks, G. W.; Schlegel, H. B.; Scuseria, G. E.; Robb, M. A.; Cheeseman, J. R.; Scalmani, G.; Barone, V.; Mennucci, B.; Petersson, G. A.et al. *Gaussian 09*, revision D.01; Gaussian, Inc.: Wallingford, CT, 2013.

(27) Frisch, M. J.; Trucks, G. W.; Schlegel, H. B.; Scuseria, G. E.; Robb, M. A.; Cheeseman, J. R.; Scalmani, G.; Barone, V.; Petersson, G. A.et al. *Gaussian 16*, revision A.03; Gaussian, Inc.: Wallingford, CT, 2016.

(28) Schlegel, H. B.; Millam, J. M.; Iyengar, S. S.; Voth, G. A.; Daniels, A. D.; Scuseria, G. E.; Frisch, M. J. Ab initio Molecular

Aerodynamics: Propagating the Density Matrix with Gaussian Orbitals. *J. Chem. Phys.* **2001**, *114*, 9758−9763.
(29) Iyengar, S. S.; Schlegel, H. B.; Millam, J. M.; Voth, G. A.; Scuseria, G. E.; Frisch, M. J. Ab initio Molecular Dynamics: Propagating the Density Matrix with Gaussian Orbitals. II. Generalizations based on Mass-weighting, Idempotency, Energy Conservation and Choice of Initial Conditions. *J. Chem. Phys.* **2001**, *115*, 10291−10302.
(30) Schlegel, H. B.; Iyengar, S. S.; Li, X.; Millam, J. M.; Voth, G. A.; Scuseria, G. E.; Frisch, M. J. Ab initio molecular dynamics: Propagating the Density Matrix with Gaussian Orbitals. III. Comparison with Born-Oppenheimer Dynamics. *J. Chem. Phys.* **2002**, *117*, 8694−8704.
(31) Chai, J.-D.; Head-Gordon, M. Systematic Optimization of Long-Range Corrected Hybrid Density Functionals. *J. Chem. Phys.* **2008**, *128*, No. 084106.
(32) Snow, K. B.; Thomas, T. F. Mass Spectrum, Ionization Potential, and Appearance Potentials for Fragment Ions of Sulfuric Acid Vapor. *Int. J. Mass Spectrom. Ion Processes* **1990**, *96*, 49−68.
(33) Brown, R. S. A Photoelectron Investigation of the Peroxide Bond. *Can. J. Chem.* **1975**, *53*, 3439−3447.
(34) Zobel, J. P.; Nogueira, J. J.; Gonzalez, L. Finite-temperature Wigner phase-space sampling and temperature effects on the excited-state dynamics of 2-nitronaphthalene. *Phys. Chem. Chem. Phys.* **2019**, *21*, 13906−13915.
(35) Benitez, Y.; Lu, D.; Lunny, K. G.; Li, J.; Guo, H.; Continetti, R. E. Photoelectron-Photofragment Coincidence Studies on the Dissociation Dynamics of the OH-CH4 Complex. *J. Phys. Chem. A* **2019**, *123*, 4825−4833.


https://doi.org/10.1021/acsomega.2c02730
*ACS Omega* 2022, 7, 33866−33872